Seabed reflection measurement uncertainty

Charles W. Holland[a)]
Applied Research Laboratory, The Pennsylvania State University, State College, Pennsylvania 16804

(Received 31 December 2002; accepted for publication 14 July 2003)

The seabed reflection coefficient is a fundamental property of the ocean waveguide. Measurements of the frequency and angular dependence of the reflection coefficient can provide information about the geoacoustic properties of the seabed or can be used as an input to propagation models. The uncertainty of the measurements must be known in order to determine prediction uncertainties for the acoustic field and/or the geoacoustic properties. Analysis indicates that the reflection measurements have a standard deviation from ± 0.5–1 dB at full angular resolution depending on frequency and experiment geometry. The dominant contribution to the error is source amplitude variability, and a new processing approach was developed that reduces the error for frequencies above a few hundred Hz. Further reduction in the uncertainty can be obtained by averaging in angle, for example, a $\pm 1°$ angle averaging leads to a standard deviation of less than ± 0.5 dB. Errors in the angle estimate are a few tenths of a degree from 0–34° grazing angle: the crucial angular range for predicting long-range propagation or for geoacoustic property inversion. [DOI: 10.1121/1.1605388]

PACS numbers: 43.30.Ma, 43.20.El, 43.30.Xm [WLS]

I. INTRODUCTION

Acoustic interaction with the seafloor often dominates and controls propagation and reverberation in continental shelf environments (e.g., Urick, 1970; Jensen and Kuperman, 1983; Eller and Gershfeld, 1985). Despite the availability of high-fidelity models (e.g., Porter, 1991; Collins, 1993; Weinberg and Keenan, 1996), acoustic predictions may have large error bars because the seafloor geoacoustic data required to drive the models have large uncertainties (e.g., Ferla and Jensen, 2002). The impact of seabed variability on acoustic predictions can be studied by analyzing fundamental acoustic measures that control seabed interaction: the seabed reflection coefficient and scattering strength. These two quantities, in principle, permit study of the seafloor independent of oceanographic variability. In this study, uncertainties associated with the reflection coefficient are examined.

Many existing techniques to estimate shallow-water seabed properties, or equivalently the seabed reflection coefficient, measure long-range propagation (e.g., Rubano, 1980; Frisk and Lynch, 1984; Beebe and Holland, 1986; Collins *et al.*, 1992; Chapman *et al.*, 2001). These techniques and similar generally spatially average over km to tens of km. A recently developed local measurement technique for reflection (Holland and Osler, 2000) averages over a much smaller footprint, ~100 m, permitting the spatial variability in the vertical and horizontal to be probed at much higher resolution. In addition, problems of intermingled geoacoustic variability with spatial-temporal oceanographic variability in long-range measurements (e.g., Siderius *et al.*, 2001) are greatly diminished because of the short distances and the short time interval over which the local measurements occur.

The reflection measurements can be used as "ground truth" for long-range methods or to extract sediment geoacoustic properties, such as sound speed, attenuation, and density. In both cases, errors associated with the reflection data are required. The objective of this research is to quantify the uncertainty associated with the direct path reflection technique.

Uncertainty or error analysis is important for several reasons. First, it is necessary in order to generally interpret the results. For example, if the data are employed to estimate seabed geoacoustic parameters, the uncertainty of the reflection data must be known in order to predict the uncertainty in the resulting geoacoustics. Second, a careful error analysis can sometimes (as it does here) point to ways in which the error can be reduced.

In any experiment the total error is a combination of the random or precision error and the systematic or bias error. The approach to error estimation taken here is two-pronged. First, the error is treated analytically and the uncertainty is derived where possible from known and estimated distributions of the measurement error. This analysis gives the random or precision error. Second, the measurement error is analyzed experimentally, i.e., by comparing multiple measurements made at nearly the same location. These two complementary approaches give a consistent picture of the uncertainty in the reflection measurements and roughly correspond to Secs. III and IV, respectively.

II. THE MEASUREMENT TECHNIQUE

The measurement technique is reviewed first, followed by pertinent details regarding the data processing. Measurements have been conducted at a wide variety of seabed types in the Mediterranean Sea and the North Atlantic Ocean. Measurements referred to in this paper were conducted on the North Tuscany Shelf, NTS, and the Malta Plateau, MP (see Fig. 1).

[a)]Electronic mail: holland-cw@psu.edu

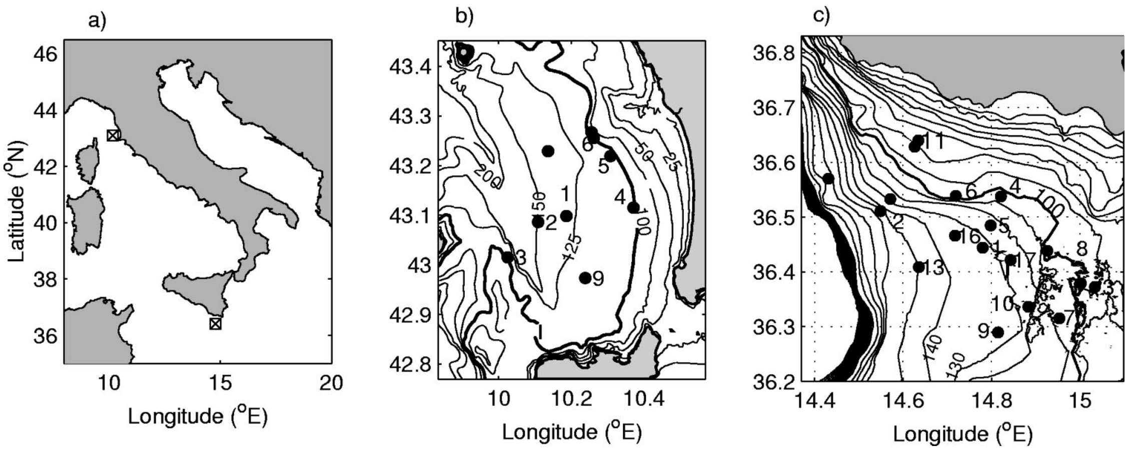

FIG. 1. Location of measurements employed to examine uncertainty in the reflection loss measurements (a) Italian littoral region, the two sites are marked by ⊗; (b) North Tuscany shelf; and (c) Malta Plateau.

A. Measurement geometry

The measurement geometry was specifically designed for shallow water, but could also be used in deep water (see Fig. 2). A broadband source is towed close to the surface, typically at a depth of a few tens of cm, and a fixed single receiver is placed far enough away from the seabed to prevent interference from the direct- and bottom-reflected paths. One of the challenges in making single bounce reflection measurements in shallow water is the presence of multipath. Towing the source close to the surface has the advantage that the surface-reflected multipaths arrive very close in time and angle and thus do not degrade the ability to associate time, range, and angle. At least two disadvantages of a near-surface source are that the surface is always changing, and that small changes in source depth can have relatively large impact on source spectrum.

Two geophysical sources have been used in the experiments, an EG&G model 265 Uniboom prior to 1999 and a GeoAcoustics model 5813B Geopulse boomer after 1999 (see Table I). The sources are metal plates driven with a high-energy impulsive signal resulting in a beam pattern similar to piston source. Pulse repetition rate was generally 1 pulse per second. Both source trigger and data acquisition were controlled by the same GPS clock to eliminate synchronization problems. The tow speed is typically about 4 knots.

The receiver and acquisition configuration has also varied over the experiments (see Table I). Prior to May 1999, a 12-bit A/D converter was used that required manual gain changes as a function of source–receiver offset in order to avoid clipping of the direct path. Subsequently, a 20-bit A/D converter was employed, eliminating the need for gain changes. The data in all experiments were telemetered to the R/V ALLIANCE via radio link. Other details about the experiment geometry can be found in Holland and Osler (2000).

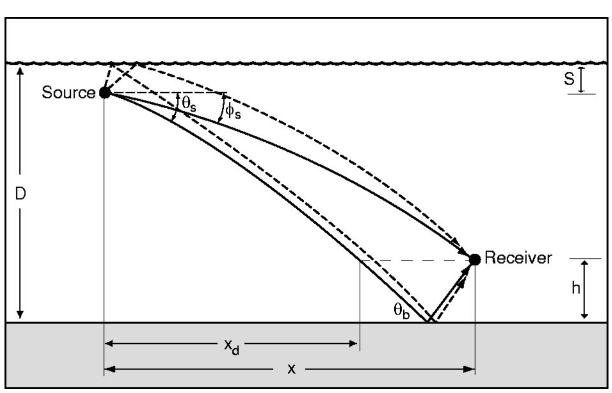

FIG. 2. Measurement geometry showing the direct and bottom bounce path ray paths along with the associated surface reflections.

B. Reflection processing

The magnitude of the pressure reflection coefficient can be defined as

$$|R(\theta_b,f)|=\left|\frac{p_r(x,f)}{p_o(x,f)}\right|, \tag{1}$$

where p_r is the received pressure from the bottom-reflected path at range x and p_o is the received level of a bottom-reflected path at x for a perfectly reflecting half-space (see Fig. 2 for measurement geometry). The denominator is written as

$$|p_o(x,f)|=|p_s(\theta_s,f)|\gamma_o, \tag{2}$$

where p_s is the source pressure amplitude at 1 m from the source, γ_o is the transmission factor from source to receiver along the bottom-reflecting path including the effects of spreading, refraction, and absorption, multiple paths (i.e., surface path), and bottom reflection (which for a perfectly reflecting bottom is unity). If the source were omnidirectional, p_s could simply be obtained measuring the pressure amplitude of the direct path at ϕ_s and correcting it back to the source. However, since the source is directional, the direct path amplitude at the same angle must come from a different range, x_d

$$|p_s(\theta_s,f)|=q_d(x_d,f)\gamma_d^{-1}, \tag{3}$$

where q_d is the amplitude of the direct path at launch angle θ_s and height h. The finite range interval of the measurements (approximately 2 m) means that in practice q_d is interpolated rather than measured directly. γ_d is the transmission factor from source to receiver along the direct path

TABLE I. List of reflection experiments with source and receiver characteristics. NTS is the northern Tuscany shelf; MP is the Malta Plateau; NJS is the New Jersey Shelf and SS in the Scotian Shelf. *El* is number of elements in the receiver string and *fs* is sampling frequency.

Cruise	Location	Date	Source	Receiver
SCARAB97	NTS	June 97	EG&G	16 *el*, 12 bit, $fs=24$ kHz
SCARAB98	MP	April 98	EG&G	16 *el*, 12 bit, $fs=24$ kHz
Boomer99	NTS	January 99	GeoAcoustics	4 *el*, 12 bit, $fs=48$ kHz
Malta99	MP	May 99	GeoAcoustics	4 *el*, 20 bit, $fs=48$ kHz
Geoscat99	NTS	October 99	GeoAcoustics	4 *el*, 20 bit, $fs=48$ kHz
Boundary00	MP	April 00	GeoAcoustics	4 *el*, 20 bit, $fs=48$ kHz
GeoClutter	NJS	April 01	GeoAcoustics	4 *el*, 20 bit, $fs=48$ kHz
Boundary01	NJS, SS	May 01	GeoAcoustics	4 *el*, 20 bit, $fs=48$ kHz
Boundary02	MP	May 02	GeoAcoustics	4 *el*, 20 bit, $fs=48$ kHz

including the effects of spreading, refraction, absorption, and multipath.

Thus, the expression for the reflection coefficient is

$$|R(\theta_b,f)|=\frac{|p_r(x,f)|}{q_d(x_d,f)}\,\frac{\gamma_d}{\gamma_o}, \tag{4}$$

where the first factor is a ratio of measured and interpolated pressures and the second factor is a ratio of modeled transmission factors. It will be convenient to refer to these two ratios in the following analysis as the ‘‘pressure ratio’’ and ‘‘transmission ratio,’’ respectively.

III. UNCERTAINTY ANALYSIS

The propagation of errors in the data processing and in the geometric factors that produce uncertainty in angle are computed using a Taylor series expansion around the mean values (Bevington and Robinson, 1992).

A. Uncertainties associated with transmission factor

The transmission ratio of Eq. (4) has uncertainties associated with the modeling of the transmission factors for the direct- and the bottom-reflected paths, which are a function of the experiment geometry. The uncertainties in the experiment geometry come from uncertainties in source depth, receiver depth, water depth, and range. We assume that errors in the model itself (Westwood, 1987) are small with respect to the errors in the geometry and thus can be neglected.

In the data processing, the transmission ratio is computed using the measured ocean sound profile and attenuation. However, in order to estimate errors, the analysis is simplified using a lossless isovelocity profile, where the transmission ratio can be written independent of range (or angle) as

$$\frac{\gamma_d}{\gamma_o}=(D-S-h)^{-1}\frac{[(D-S+h)^2+x^2]^{1/2}}{[1+x^2(D-S+h)^{-2}]^{1/2}}=\frac{D-S+h}{D-S-h}, \tag{5}$$

where D is water depth, S is source depth, and h is receiver height above the seafloor (see Fig. 2). The attenuation is ignored for the error analysis because its contribution is small (less than 3%) even at the highest frequency, 10 kHz, and longest range, 1 km.

Water depth is measured acoustically using a 12-kHz fathometer, a swath mapping system, and/or the near-normal

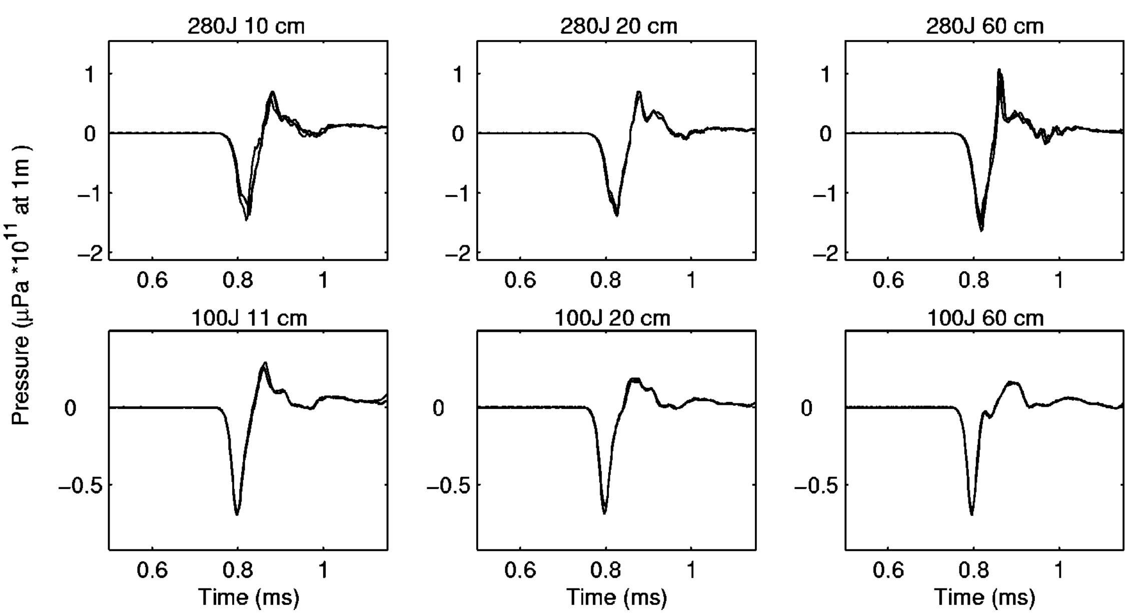

FIG. 3. Tank measurements of GeoAcoustics boomer at various energy levels (280 and 100 joules) and source depths at normal incidence. Each panel has three pulses.

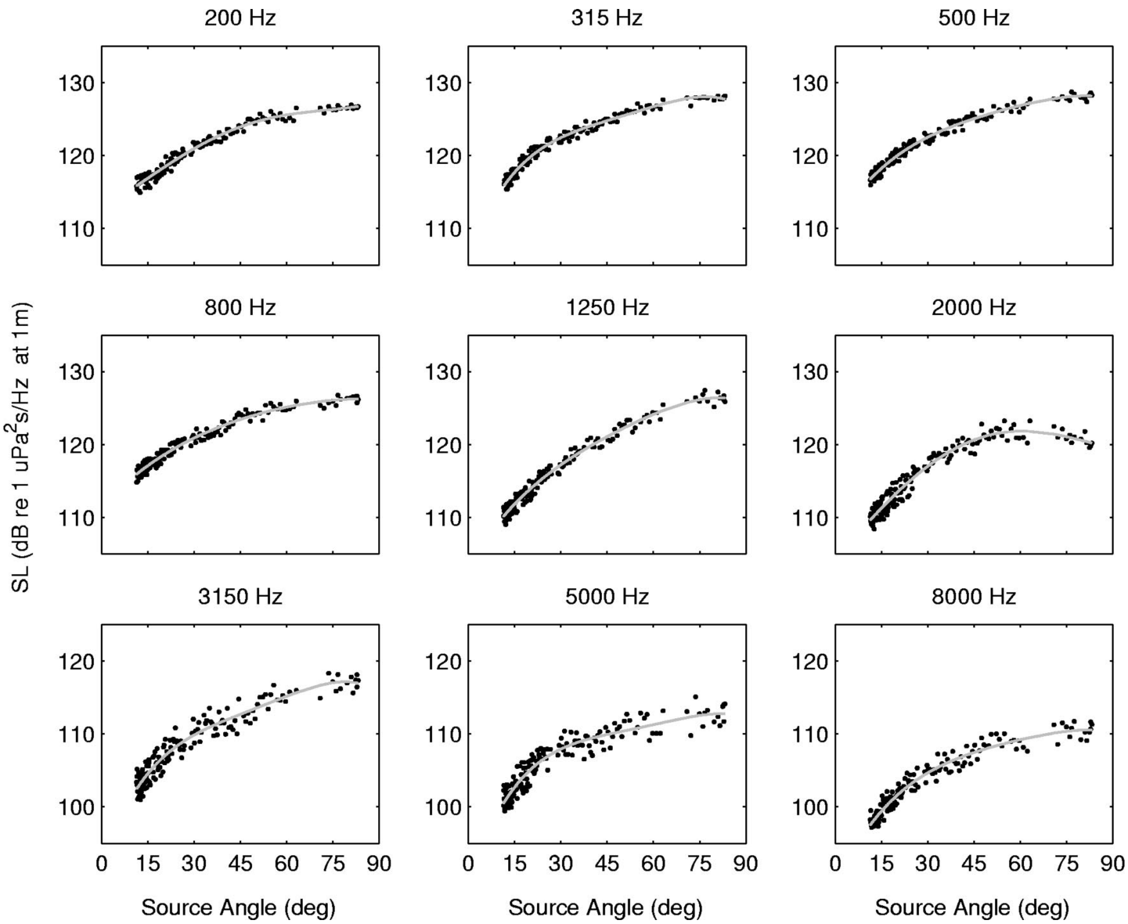

FIG. 4. Energy spectral density source level measurements (●) with polynomial fits (gray line) for various 1/3-octave frequency bands at MP site 7.

incidence bottom reflection on an array towed near the source. This estimate has a standard deviation of order a few tens of cm. The greater source of error for *D* occurs because the source is mounted on a surface-towed catamaran, so that the effective water depth varies with the passing waves, which may be up to of order 1 meter. The variability associated with *S*, which has a mean depth of 0.35 m, is associated with the nonconstant drag forces on the catamaran including small changes in instantaneous ship speed, wake turbulence, unsteady surface currents, and surface waves. It is believed that instantaneous changes in ship speed and wake effects dominate the variability in *S*. Receiver height is measured onboard before deployment; the length of the Kevlar rope attached to the sea anchor fixes its height. Receiver height errors occur because of rope stretching (presumed very small for Kevlar), displacement due to currents, and sinking of the sea anchor into the seabed.

Assuming that the errors in water depth, source depth, and receiver height are independent (which seems reasonable given that the processes that govern them are independent), the standard deviation, σ_t, associated with the transmission ratio [Eq. (5)] can be written

$$\sigma_t = ((\sigma_D^2 + \sigma_S^2)(1-\mu_t)^2 + \sigma_h^2(1+\mu_t)^2)^{1/2} \times (\mu_D - \mu_S - \mu_h)^{-1}, \tag{6}$$

where μ_t is the mean transmission factor. For reasonable mean and standard deviations ($\mu_D = 120$ m, $\mu_S = 0.35$ m, $\mu_h = 15$ m, $\sigma_D = 1$ m, $\sigma_S = 0.25$ m, $\sigma_h = 0.3$ m) the resulting relative errors are less than 1%, or 0.05-dB absolute error.

B. Uncertainties associated with the source level

The pressure ratio of (4) has no uncertainty associated with the calibration, since the bottom-reflected signal and the direct path signal are influenced by the hydrophone calibration and receiving electronics in precisely the same way.

However, the pressure ratio has uncertainty associated with the source amplitude and is the major contribution to the error budget. The source amplitude variability comes from two factors: (1) inherent variability in the drive voltage and the source plate response, and (2) nonconstant drag forces on the catamaran (caused by small changes in ship speed/direction, wake turbulence, and passing waves), which result in variability of the source plate depth and angle from ping to ping. Tank measurements of the source show it to be highly repeatable (see Fig. 3). Therefore, the largest contribution to the error is source variability due to motion. While small variations in source plate depth (a few tens of cm) played a nearly insignificant role for the transmission factor, they can lead to significant variations in amplitude (a few dB) both because of the sensitivity of plate response to hydrostatic pressure and sensitivity of the received pressure to the sea surface multipath.

Figure 4 shows 1/3-octave averaged source measurements at various frequencies along with the fitted polynomi-

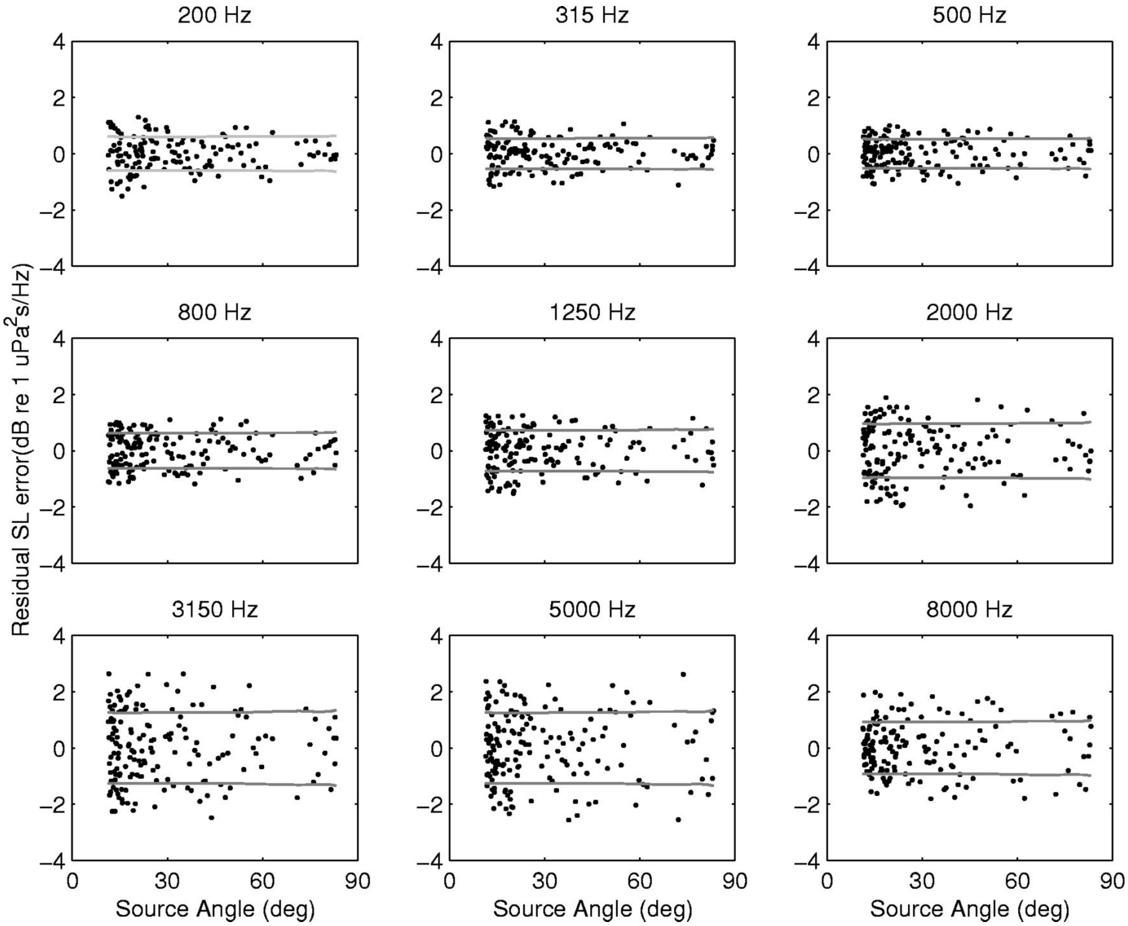

FIG. 5. Residual error (●) associated with polynomial fits of Fig. 3 with standard deviation (gray line) at MP site 7.

als. The data have been screened for signal-to-noise ratios greater than 6 dB, and outliers (greater than 2σ) have been removed. The residual errors of the polynomial fits are shown in Fig. 5. Note that the errors appear to be random, which means that the polynomial fit is appropriate. The distribution of the errors is approximately Gaussian. The standard deviations of the fits are relatively independent of angle but are dependent upon frequency ranging from a minimum of 0.5 dB at low frequencies to a maximum of 1.4 dB at 5000 Hz (see Fig. 6). Although these are reasonably typical, the frequency dependence of the standard deviation varies from run to run. As a general rule, the standard deviation is proportional to sea state: the higher the sea state, the larger the deviation. Measurements are generally conducted in sea state 3 or less. Assuming that the variability at ranges x and x_d are uncorrelated, the standard deviation in the reflection coefficient ranges from about 1–2 dB, depending on frequency.

C. Source variability normalization

While the errors associated with the data processed by Eq. (4) are reasonably small, error analysis suggested a novel way to reduce the error associated with source variability. If the source variability is predominantly due to amplitude fluctuations rather than beam-pattern fluctuations (e.g., caused by source plate tilt), then the variability can be reduced by normalizing by the same ping for the direct path as the bottom-reflected path and correcting by the ratios of the fitted average

$$|p_s(\theta_s,f)| = |p_d(x,f)|\,\frac{q_d(x_d,f)}{q_d(x,f)}\,\gamma_d^{-1}. \tag{7}$$

Now the reflection coefficient becomes

$$|R(\theta_b,f)| = \left|\frac{p_r(x,f)}{p_d(x,f)}\right|\frac{q_d(x,f)}{q_d(x_d,f)}\,\frac{\gamma_d}{\gamma_o}, \tag{8}$$

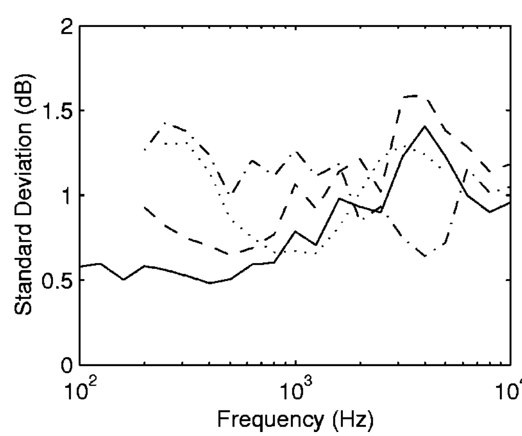

FIG. 6. Standard deviation of source level fits: MP site 7 (solid), an example from a single run in 1998 (dotted), 2000 (dashed), 2002 (chain dashed).

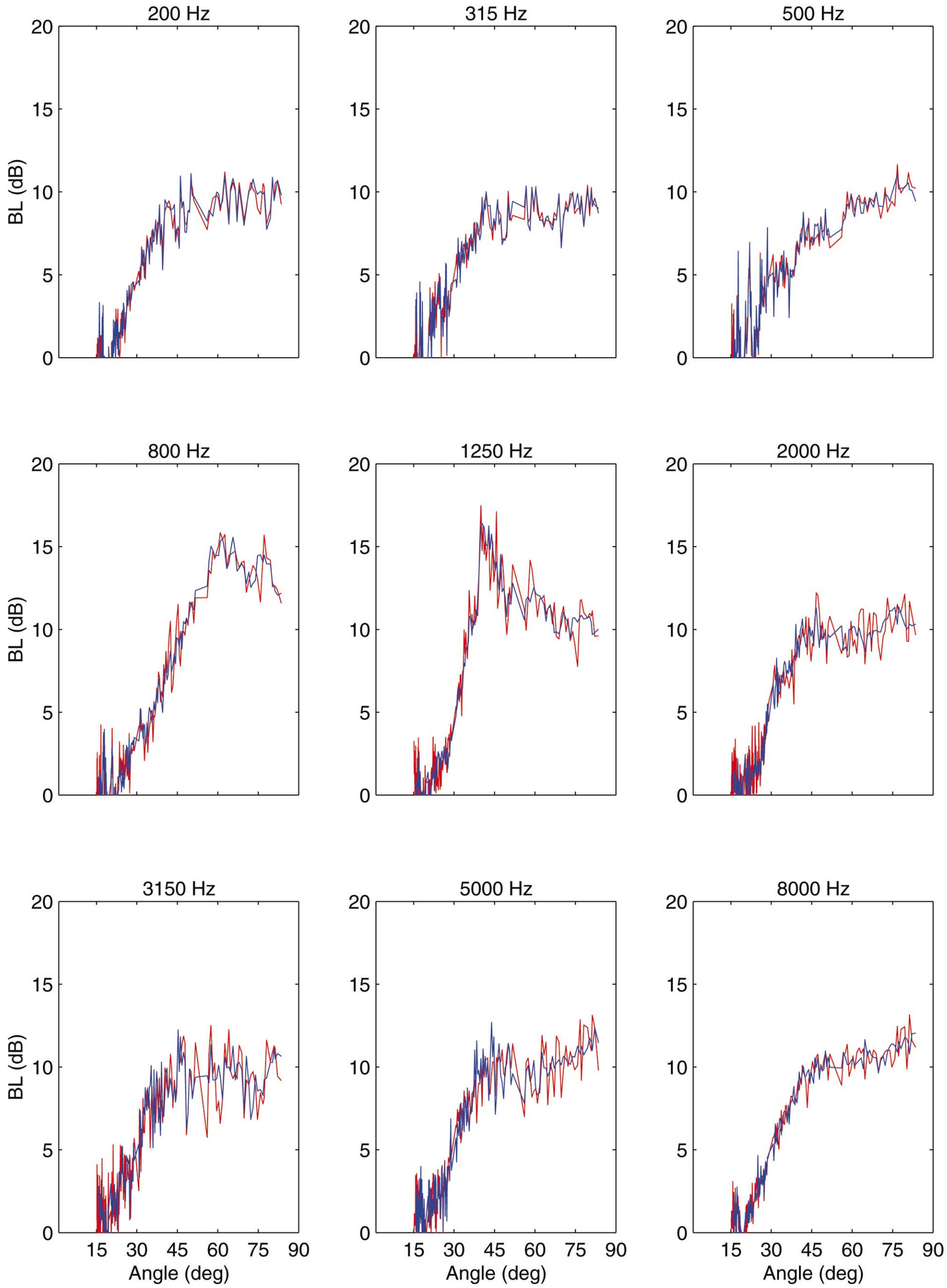

FIG. 7. Results of processing with Eq. (4) (red) and Eq. (8) (blue) at MP site 7; note the decrease in the fluctuations, especially above 800 Hz. The source level data are from Fig. 3.

where the first factor is a ratio of measured pressures for the same ping, so that ping-to-ping amplitude variability is completely normalized. In this form, the variability of the reflection coefficient only depends upon the variability in the fitted source level and thus should be about 0.5–1.5 dB (see Fig. 6).

The form of Eq. (8) requires no more computational load, and provides a fully normalized reflection coefficient. If there is significant ping-to-ping rotation of the source plate, then the errors associated with (8) actually are larger than (4). However, for most of the measurements conducted to date, (8) appears to reduce the error budget. As an example, Fig. 7 shows reflection data processed using Eq. (4) and Eq. (8) at MP site 7 (same site as Fig. 4). The fluctuations do appear to be smaller for (8). In order to obtain the quantitative difference in the standard deviation, the exact reflection coefficient must be known. That is, the apparent fluctuations in the reflection coefficient could be real, for example due to resonant interaction between layers, or at the higher frequencies, due to scattering. In order to estimate the change of (8), we make the assumption that the exact reflection coefficient at this site is perfectly smooth. Then, the standard deviations show that while some of the lower frequencies are degraded slightly, the midfrequency deviations are reduced (see Fig. 8). These standard deviations are an upper bound, given the foregoing assumption.

D. Angle uncertainty and resolution

The first step in determining the angle uncertainty is to determine the uncertainty in range. In the data processing, range is estimated by fitting modeled (Westwood, 1987) to

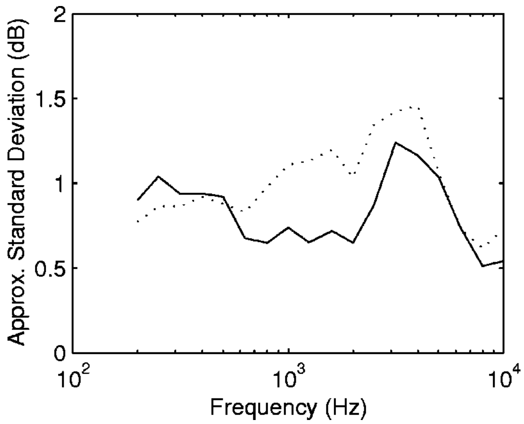

FIG. 8. Effect of source amplitude normalization; Eq. (4) (dotted) and Eq. (8) (solid). Bottom angles from 25–90° are included in the statistics.

measured arrival times, which are obtained by amplitude thresholding the direct path arrival. Although the measured sound-speed profile is used in the data processing, an isovelocity profile is used to simplify the error analysis. Thus, range, x, and its standard deviation are given by

$$x=\left|(c\tau)^2-(D-S-h)^2\right|^{1/2}, \tag{9}$$

$$\sigma_x=\mu_x^{-1}[\mu_c^2\mu_\tau^2(\sigma_\tau^2\mu_c^2+\sigma_c^2\mu_\tau^2)+(\mu_D-\mu_S-\mu_h)^2 \times(\sigma_D^2+\sigma_S^2+\sigma_h^2)]^{1/2}, \tag{10}$$

where c is sound speed and τ is travel time of the direct path. Sound speed is measured generally with a CTD and XBT; a reasonable estimate of the standard deviation from these instruments is $\sigma_c=0.25$ m/s. An estimate of the standard deviation in the direct arrival is $\sigma_\tau=0.1$ ms or about 1 pulse width (see Fig. 3). Assuming the same means and standard deviations as in Sec. III A, the resulting mean and standard deviation of the range are shown in Fig. 9. Note that near normal incidence, there is a bias error in the mean range (9) and that the standard deviation (10) becomes infinite. Near normal incidence $(x\rightarrow 0)$, the mean and standard deviation can be estimated as

$$\mu_{x=0}\approx 2^{1/4}[\mu_c^2\mu_\tau^2(\sigma_\tau^2\mu_c^2+\sigma_c^2\mu_\tau^2)+(\mu_D-\mu_S-\mu_h)^2 \times(\sigma_D^2+\sigma_S^2+\sigma_h^2)]^{1/4}, \tag{11}$$

$$\sigma_{x=0}\approx \tfrac{1}{2}[\mu_c^2\mu_\tau^2(\sigma_\tau^2\mu_c^2+\sigma_c^2\mu_\tau^2)+(\mu_D-\mu_S-\mu_h)^2 \times(\sigma_D^2+\sigma_S^2+\sigma_h^2)]^{1/4}. \tag{12}$$

The angle at the seabed, θ, and its associated standard deviation (in radians) are given by

$$\theta=\tan^{-1}((D-S+h)/x), \tag{13}$$

$$\sigma_\theta=\mu_x^{-1}\cos^2\mu_\vartheta(\sigma_D^2+\sigma_S^2+\sigma_h^2+\sigma_x^2\tan^2\mu_\vartheta)^{1/2}. \tag{14}$$

At normal incidence (i.e., $\theta=\pi/2$) the mean angle and the standard deviation (13)–(14) have bias errors, but can be estimated as

$$\mu_{\vartheta=\pi/2}=\tan^{-1}((\mu_D-\mu_S+\mu_h)/\mu_{x=0}), \tag{15}$$

$$\sigma_{\vartheta=\pi/2}=\sigma_{x=0}(\mu_D-\mu_S+\mu_h)^{-1}. \tag{16}$$

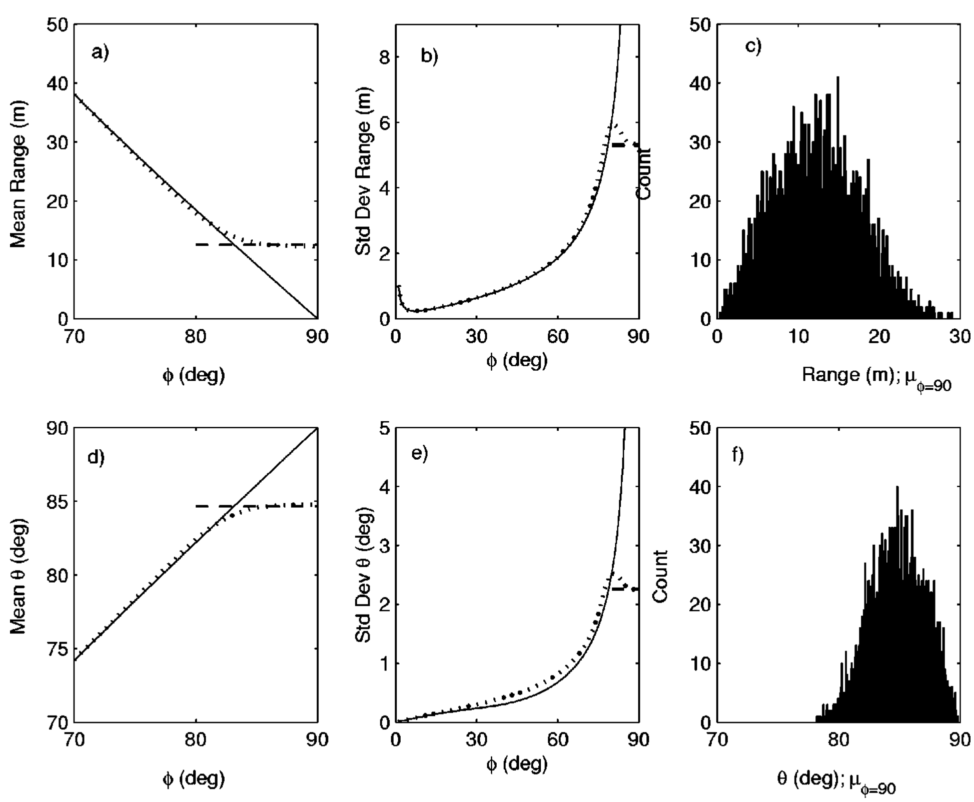

FIG. 9. Theoretical (solid), simulated (dotted line) and approximate (dashed line) solutions for: (a) mean of range estimate, Eq. (9) is solid line, Eq. (11) is dashed line; (b) standard deviation of range estimate, Eq. (10) is solid line, Eq. (12) is dahsed line; (d) mean of angle estimate, Eq. (15) is dashed line; (e) standard deviation of angle estimate, Eq. (14) is solid line, Eq. (16) is dashed line. The histograms show simulation results at normal incidence for (c) range and (f) angle estimates.

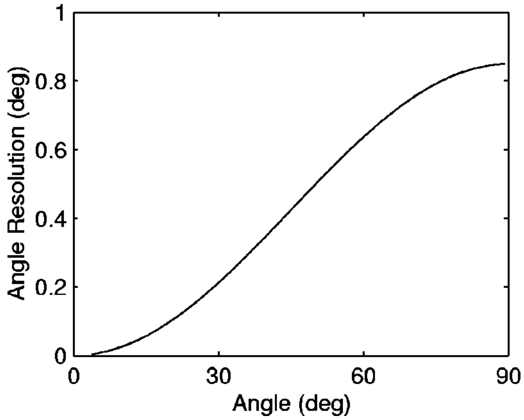

FIG. 10. Typical angular resolution of the reflection measurements.

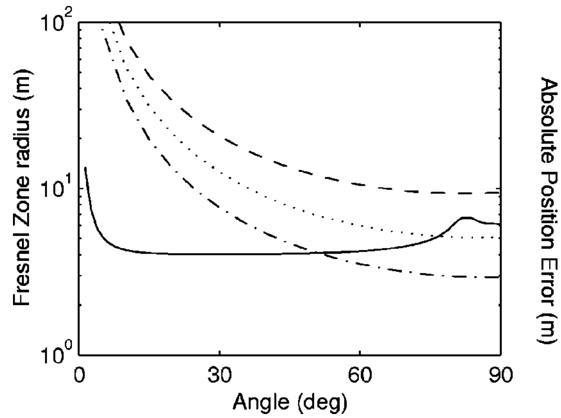

FIG. 11. Absolute position error (solid line) for a source, receiver 120 and 15 m above the seabed, respectively, and the Fresnel zone radius 300 Hz (dashed), 1000 Hz (dotted), and 3000 Hz (chain dashed).

The part of the angular range that is the most crucial for minimizing errors is dictated by where the critical angle or angle of intromission is expected, since these angles control long-range propagation. Hamilton (1980) indicates that for unconsolidated sediments on the continental shelf, critical angles vary from 0–34°. In that range the standard deviation of the angle uncertainty is quite small, from about 0.01–0.3°. At normal incidence, the errors are considerably larger; however, the increase in errors is mitigated, in part, by the fact that the reflection coefficient itself is often nearly constant between 70–90° (e.g., Fig. 7).

The angular resolution (difference in angle between two adjacent measurements) is a function of the ship speed ν, pulse repetition rate ϖ, and the geometry. Since the pulse repetition rate is constant, the resolution δ_θ is a function of angle. For an isovelocity sound-speed profile, the angle resolution is

$$\delta_\vartheta = \nu \varpi \mu_x^{-1} \cos^2 \mu_\vartheta((\mu_D - \mu_S + \mu_h)/\mu_x). \tag{17}$$

Given typical parameters, $\nu = 2$ m/s and $\varpi = 1$ pulse per s, with the geometry as above, the angular resolution is less than 1° (see Fig. 10).

E. Absolute position uncertainty

A reflection experiment yields four measurements around the fixed receiver, typically two aligned with the bathymetric contours (i.e., an incoming and an outgoing), and two perpendicular. The region of the bottom that is sampled by each measurement depends on water depth, sound-speed profile, and receiver depth, but generally ranges from about 70–150 m in length. The uncertainty of the absolute position of each measurement is due to uncertainty in the location of the fixed receiver and location of the source.

The location of the receiver is determined by a least-squares fit to echolocation data. Transponders operating at 9–11 kHz mounted on the hull of the ship and on the fixed hydrophone string a few meters above the bottom provide the echolocation data. A typical echolocation run consists of an "x" pattern, attempting to place the center of the "x" as close as possible to the location of the drop position of the array. The least-squares fit to a model assuming straight-line ray paths gives fits of ± 2–7 m depending on how close the estimated drop position was to the actual hydrophone position. In addition, there is a ± 2–3-m uncertainty in the differential GPS (DGPS) estimate, so that the receiver position is generally known to within ± 3–8 m. The isovelocity approximation for the echolocation data is reasonable since the transponder data are generally at grazing angles greater than about 30 deg.

The source is towed from a crane. The position uncertainty of the source relative to the ship is about ± 2 m, and with the DGPS uncertainty of ± 2–3 m, the overall source position accuracy is about ± 4 m. Since range is estimated acoustically and is more precise than the positions, and source position standard deviation, σ_{sp}, is less than that of the receiver, the source position and the range is used to estimate absolute position. The standard deviation of the absolute position is

$$\sigma_L = (\sigma_{sp}^2 + (\sigma_D^2 + \sigma_S^2)\tan^{-2}\theta + \sigma_\theta^2(\mu_D - \mu_S)^2 \sin^{-4}\theta)^{1/2}. \tag{18}$$

The absolute positional uncertainty should be considered in light of the size of the region on the seabed illuminated by the acoustic field. The radii of the first Fresnel zone (see Fig. 11) are useful metrics for estimating that size. In Fig. 11, the larger radius of the Fresnel ellipse was used (in the plane of the source–receiver). Note that the positional errors are of the same order or smaller than the Fresnel zone radius except at high frequencies and high angles.

F. Other errors

There is another potential source of error that may contribute to the reflection coefficient related to assumptions inherent in the measurement and data processing. It is implicitly assumed that the bathymetry, sediment layer geometry, and sound velocity profile are independent of space (several hundred meters) and time (5–10 min) during the measurement. Bathymetry and normal incidence seismic reflection data are always collected and analyzed to ensure that the first two assumptions are met. Generally a conductivity–temperature–depth (CTD) cast is taken before the experiment commences and an expendable bathythermograph (XBT) is collected during the actual measurement evolution near the hydrophone position. The temperature data from the

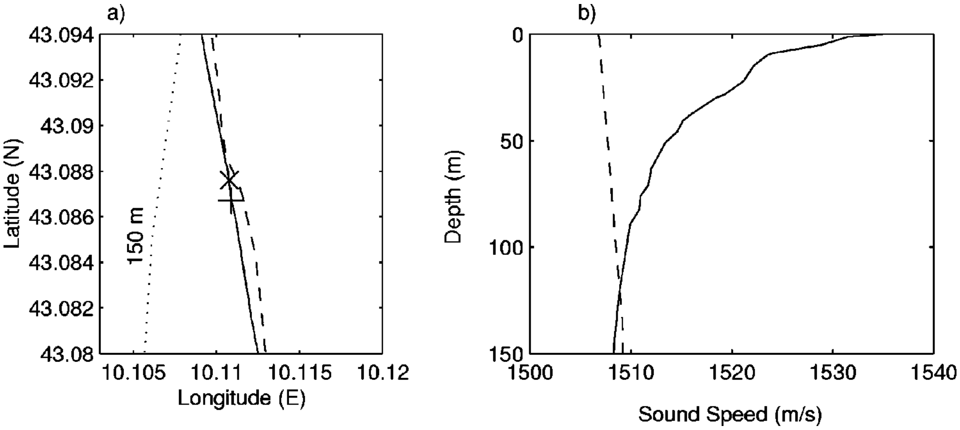

FIG. 12. NTS site 2(a) array position, for 1997 (+), 1999 (×), and reflection loss tracks 1997 (solid), 1999 (dashed) with bathymetry contour; (b) sound-speed profiles for June 1997 (solid), January 1999 (dashed).

XBT cast with the salinity data from the CTD are employed to represent the sound-speed structure over the minutes and hundreds of meters of the experiment. If sound-speed variability exists within this time/space scale, the effect would probably be a small shift in grazing angles.

IV. OBSERVED UNCERTAINTY

Multiple reflection loss measurements in the same area provide the opportunity to analyze the uncertainty from the measurement standpoint. Since the measurements are conducted under varying conditions, it is desirable to define in what sense the measurements are repeated.

Coleman and Steele (1999) draw a useful distinction between the words ''repetition'' and ''replication'' of measurements that is adopted here. Replication implies that the measurements are repeated in a particular fashion. Zeroth-order replication means that the measurements are repeated with identical instrumentation and perfectly constant experimental conditions. Only changes inherent in the source–receiver over time-space contribute to variation in the results. First-order replication means repetition with identical instrumentation but with variation in the experimental conditions, so that the observed variability in the data would be a combination of variability of the instrumentation and the conditions. *N*th-order replication is when both the instrumentation and the experimental conditions change. By completely changing both the instrumentation and the experimental conditions, *n*th-order replication permits an estimate of the total error.

In the suite of reflection measurements (Table I), there are never instances of pure replication of any order, i.e., where the same seabed is measured multiple times. There are instances, however, when nearly the same portion is measured multiple times. For example, seismic reflection data often indicate that the seabed on the ingoing and outgoing legs has a similar character. This roughly corresponds to the

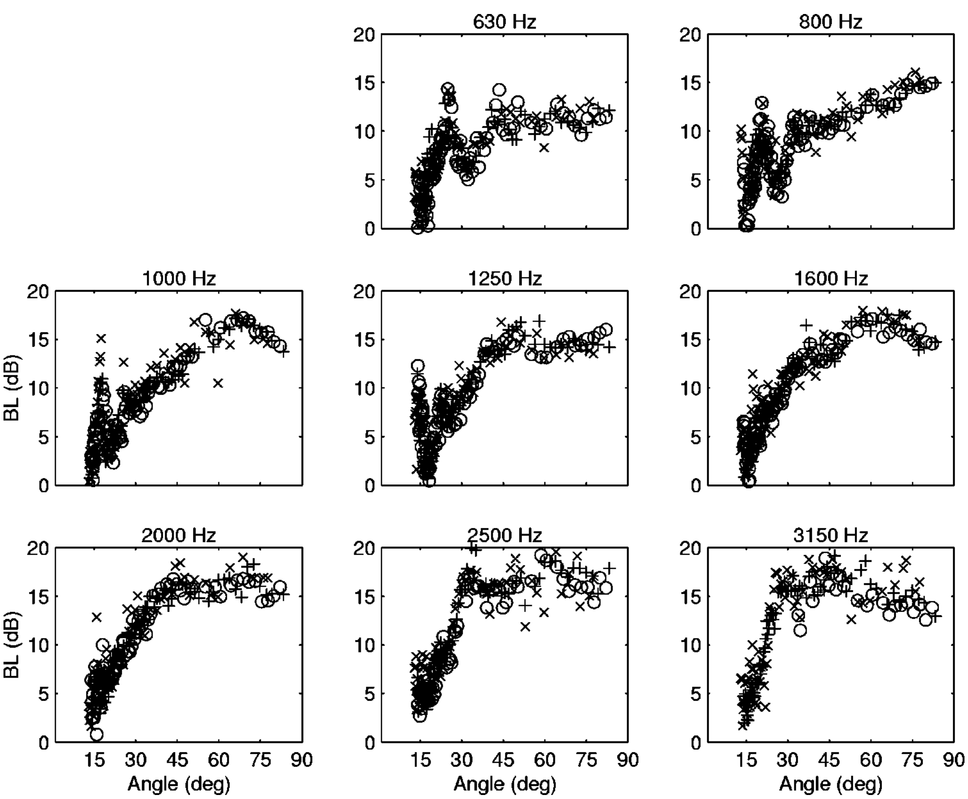

FIG. 13. Measured reflection loss at NTS site 2: south leg June 1997 (+), north leg June 1997 (○), south leg January 1999 (×).

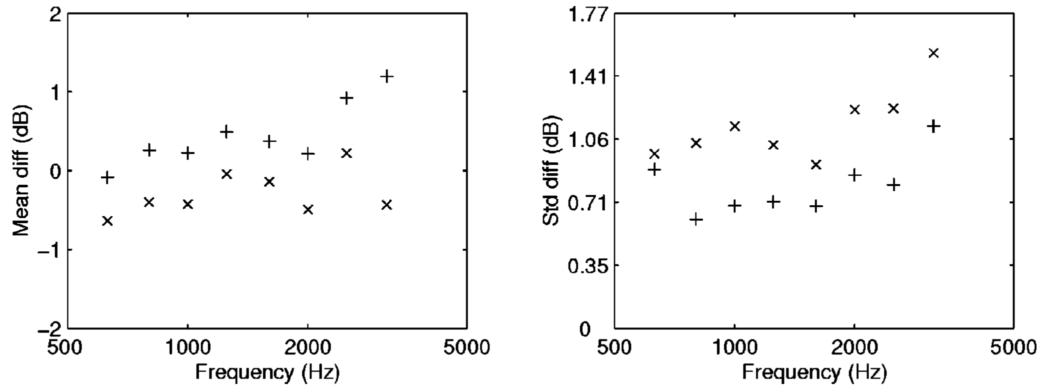

FIG. 14. NTS site 2 mean and standard deviation of the reflection loss difference: between south and north legs June 1997 (+); south leg June 1997, and south leg January 1999 (×).

first-order replication, where the source and receiver are identical, but with the passage of time between the experiments, the conditions (e.g., sound-speed profile) are allowed to vary. Actually, though the source itself is the same between the incoming and outgoing legs, the source characteristics change measurably because of an inherent tilt in the source plate, so it could be argued that this replication is nth order. Another replication is where the source and receiver are completely different, and the sound-speed profile is completely different. This roughly corresponds to the nth-order replication. In both cases the observed variance will be an outer bound because the region of sampled seabed is (slightly) different.

In order to determine if the replication results were a function of seabed type, repeated measurements were analyzed in two very distinct seabed environments: Site 2 in 150-m water depth in the North Tuscan shelf in the northern Tyrrhenian Sea (silty-clay host with random thin shelly layers), and site 7 in 107-m water depth on the Malta Plateau, Straits of Sicily (fine sand over limestone; see Fig. 1 for locations).

A. North Tuscany observations

Multiple measurements at site 2 permit comparison of reflection results under various conditions. During the SCARAB97 experiment in June 1997, measurements were conducted on a nearly N–S track. Data from the southern leg (i.e., south of the array position) were analyzed and reported in Holland and Osler (2000). Since seismic reflection data show that the layering structure changes little over the northern leg, data from the two legs can be compared. In addition, measurements were made in the Boomer99 experiment in January 1999 with the receive array 100 ± 7 m north of the 1997 array position [see Fig. 12(a)]. The source and receiver depths in 1997 were 0.35 and 138 m, and in January 1999 0.11 and 136 m. The source used in the 1997 experiment was an EG&G model 265 Uniboom and in 1999 a GeoAcoustics Uniboom with higher source level, but the shallower tow depth meant higher source level variability.

These three data sets provide the opportunity to examine the uncertainty (including the variability) over quite different experimental conditions; the sound-speed profiles for the two seasons are shown in Fig. 12(b). The reflection data in Fig. 13 show strong similarities. A statistical comparison was performed by forming the difference between data sets (after interpolation) and computing the mean and standard deviation of the difference (see Fig. 14). The mean of the data difference indicates whether or not there is a bias; the standard deviation gives an indication of the variance between the data sets. Frequently, at low angles, the data rapidly oscillate in angular increments that are at or below the uncertainty of the measurements. Out-of-phase oscillations can produce very large variances; this effect was reduced by per-

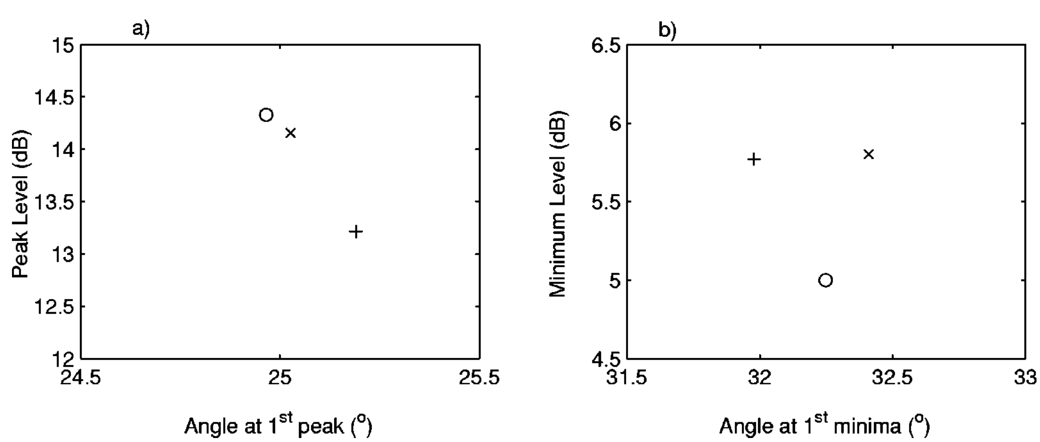

FIG. 15. Comparison of three data sets at 630 Hz for the (a) first peak and (b) first minima.

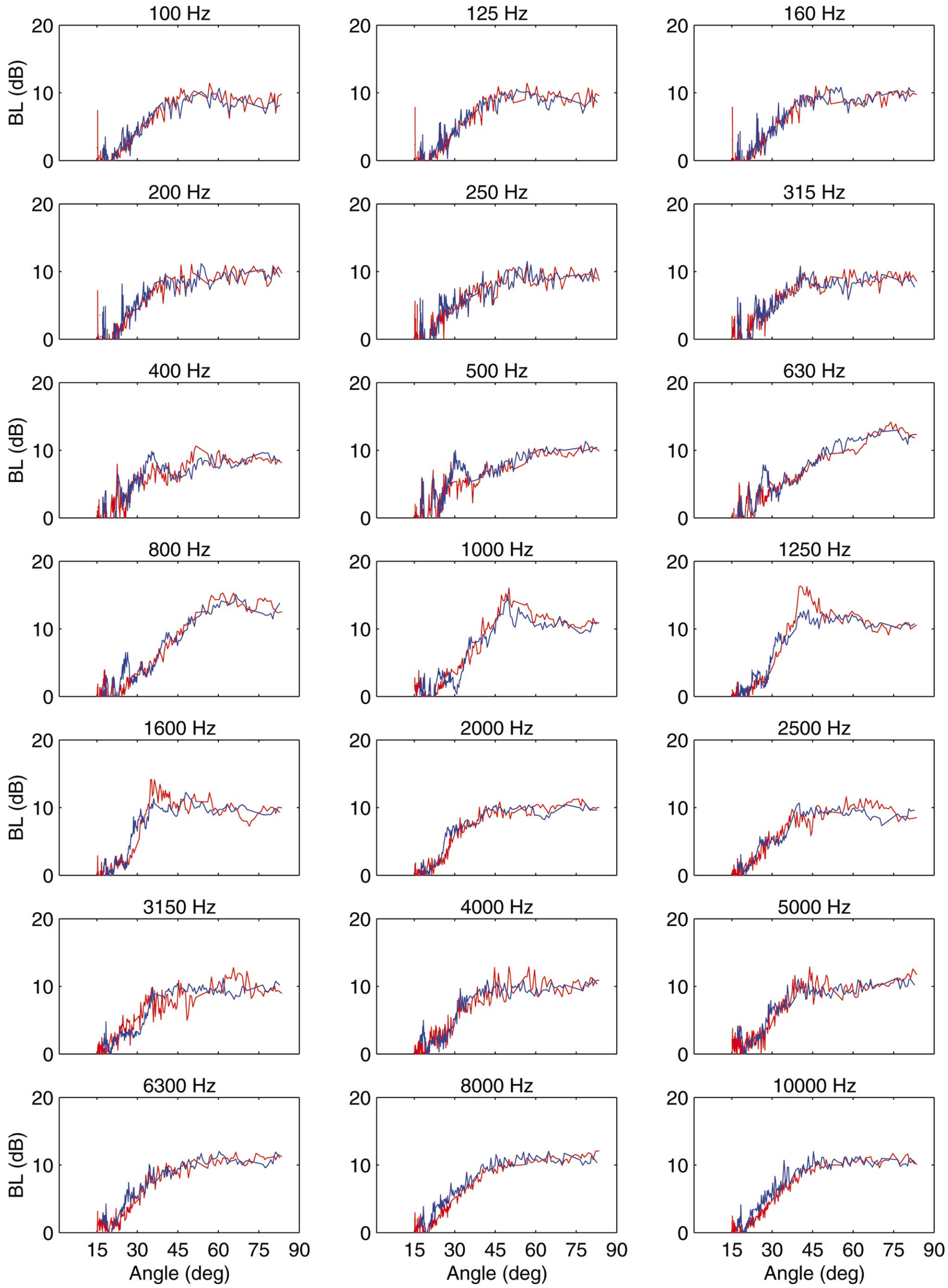

FIG. 16. MP site 7 comparison of reflection loss: south leg (red) and north leg (blue).

forming the statistics on data greater than 25°.

The mean difference between the 1997 measurements (Δ_{sn}) is about 1 dB or less (Fig. 14), with the greatest difference being at the highest frequencies. The mean difference between the 1997 and the 1999 (Δ_{ss}) measurements is also less than 1 dB. Δ_{sn} is somewhat smaller than Δ_{ss} below 2 kHz but larger above 2 kHz. The reason for this is unknown, but is probably related to the fact that the signal-to-noise ratio of the northern path was considerably smaller than that for the incoming. The important point of this figure is that the measurements are repeatable within 1 dB or less and there is no apparent consistent bias in the measurements.

The angle error inherent in the measurement predicted in Eq. (14) can be compared against the measurements by examining the angular offset between maxima (or minima) in the reflection data. The 1997 data were processed with a decimation factor of 3 (1 pulse every 3 s); the 1999 data have a decimation of 4 s. For a strict comparison, the decimation should be equal and as low as possible; however, even the data as they are permit an upper bound estimate of the error. In order to try and minimize possible differences due to spatial variability (the measurements sampled different parts of the seabed, of order 100 m apart), the lowest frequency, 630 Hz, is used for this comparison.

At 630 Hz, the first peak and minima are convenient points at which to compare the angles from the various experiments. A plot of the resulting first peak angle and first minima is shown in Fig. 15. The theory [Eq. (14)] indicates

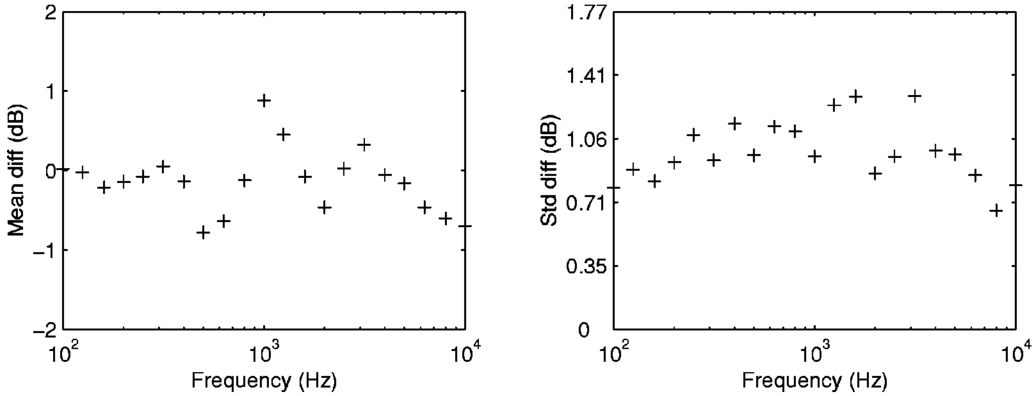

FIG. 17. MP site 7 mean and standard deviation of the reflection loss difference between the south and north legs.

that at 25°, the standard deviation $\sigma_\theta = 0.15°$ for the first peak, the observed $\sigma_\theta = 0.12°$. For the reflection loss minimum at about 32°, the theory indicates a $\sigma_\theta = 0.18°$ and the observed $\sigma_\theta = 0.22°$. Thus, the predicted angle errors seem to be quite reasonable. The site specific parameters used for the predictions were: $\mu_D = 150$ m, $\mu_S = 0.35$ m, $\mu_h = 13$ m, $\sigma_D = 1$ m, $\sigma_S = 0.25$ m, $\sigma_h = 0.3$ m, $\sigma_c = 0.25$ m/s, and $\sigma_\tau = 0.1$ ms.

The data can also be used to compare the uncertainty of the peak levels; however, this is a rather stringent test given that the amplitude of a narrow peak will not be well estimated for various sampling intervals as is the case here. Nevertheless, a comparison is useful as a guide; the standard deviation of the peaks at 25° and 32° are 0.6 and 0.5 dB, respectively, which are well within the estimated standard deviation.

B. Malta Plateau observations

Multiple reflection experiments at site 7 permit comparison at a different location. These experiments were conducted during Boundary2000 in May 2000. A combination of the source (GeoAcoustics Uniboomer) and the seabed type, thick sand over consolidated limestone, allowed a comparison over a broader frequency band than possible on the north Tuscany shelf. Figure 16 shows the reflection measurements for the southern and northern legs of the experiment. The agreement is generally good, although there are some clear differences that are believed to be due to slight differences in sediment fabric. Even including the variability due to sediment inhomogeneity, the mean difference between the two runs is quite small (Fig. 17), less than 1 dB.

V. REDUCING UNCERTAINTY

Although the uncertainty in the reflection data is modest, there are several ways in which the variance could be further reduced: by averaging in angle or by modifying the source.

A. Reducing uncertainty by averaging

Given that resolution can be traded for variance (e.g., Menke, 1989), averaging over angle space can be done to reduce the variance. As an example, the source level data of site 7 were reprocessed with a $\pm 1°$ sliding window. The resulting standard deviation, compared with the full angular resolution (see Fig. 18) is significantly reduced to ~0.1–0.5 dB.

The advantage of decreased variance may or may not offset the loss in resolution depending on the particular problem. However, given the very high resolution in angle, especially at low angles (see Fig. 10), angle averaging should provide a useful reduction in variance for many situations. Some situations suggest a strategy of a variable window size, i.e., a window that is a function of angle. For example, in obtaining geoacoustic properties in fine-grained sediments (see Holland, 2002) a low variance near 90° with a high angle resolution near the angle of intromission (in that case 15°) would yield the highest precision in the resulting velocity and density estimates. That could be easily accomplished with a large window size near 90° and a small (or zero) window near the angle of intromission. Obtaining high-precision velocity and density estimates from sandy sediments (with a critical angle) suggests a similar strategy.

B. Reducing uncertainty by modifying the source

Another way to reduce the variance would be to use an omnidirectional source, which would eliminate sensitivity to source rotation. Practically speaking this is difficult, since a large bandwidth is desirable. A sparker source was investi-

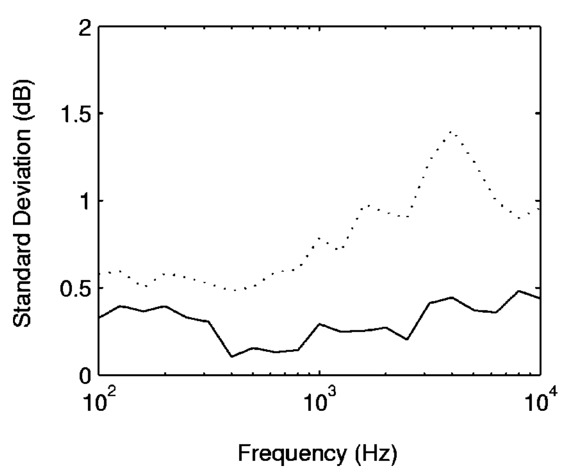

FIG. 18. Reduction in variance achieved by angle averaging: no angle averaging (dotted line) and ± 1-deg angle averaging (solid line).

gated, which has a more omnidirectional beam pattern, but the source amplitude variability was much larger than that of the Boomer.

Yet another way to diminish the errors would be to tow the source at a much greater depth. In an experiment planned in 2004, the source will be mounted on an autonomous undersea vehicle (AUV) and flown a few tens of meters above the bottom. In addition to eliminating the uncertainties due to the air–sea interface, the deep-tow geometry will substantially reduce the time required for multiple measurements.

VI. SUMMARY AND CONCLUSIONS

Error analysis of the reflection measurements has shown that standard deviations are typically ± 0.5–1 dB at full angular resolution. Averaging in angle can reduce that substantially, for example $\pm 1°$ angle averaging leads to a standard deviation of ± 0.1–0.5 dB. Specific error estimates depend upon frequency, geometry, and location. The dominant contribution to the error is source amplitude variability, and a new processing approach was developed that reduces the error for frequencies above a few hundred Hz.

Errors in the angle estimate are a few tenths of a degree below 35 deg, which is the crucial angular range for predicting long-range propagation or inverting for geoacoustic properties. The largest contribution to the error in the angle estimates comes from wave motion that induces variability in source height. Absolute position errors of the measurements are about 3–8 m.

ACKNOWLEDGMENTS

We gratefully acknowledge the support of the NATO SACLANT Undersea Research Center and the Office of Naval Research. Enzo Michelozzi conducted the tank measurements.

Beebe, J. H., and Holland, C. W. (**1986**). ''Shallow-water propagation effects over a complex, high-velocity bottom,'' J. Acoust. Soc. Am. **80**, 244–250.

Bevington, P. R., and Robinson, D. K. (**1992**). *Data Reduction and Error Analysis for the Physical Sciences*, 2nd ed. (McGraw-Hill, New York).

Chapman, R., Chin-Bing, S., King, D., and Evans, R. (**2001**). ''Benchmark workshop for geoacoustic inversion techniques in range-dependent waveguides,'' J. Acoust. Soc. Am. **110**, 2660.

Collins, M. D., Kuperman, W. A., and Schmidt, H. (**1992**). ''Nonlinear inversion of sediment parameters in a range-dependent region of the Gulf of Mexico,'' J. Acoust. Soc. Am. **92**, 2770–2783.

Coleman, H. W., and Steele, W. G. (**1999**). *Experimentation and Uncertainty Analysis for Engineers* (Wiley, New York).

Collins, M. D. (**1993**). ''A split-step Padé solution for the parabolic equation method,'' J. Acoust. Soc. Am. **93**, 1736–1742.

Eller, A. I., and Gershfeld, D. A. (**1985**). ''Low frequency acoustic response of shallow water ducts,'' J. Acoust. Soc. Am. **78**, 622–631.

Ferla, C., and Jensen, F. B. (**2002**). ''Are current environmental databases adequate for sonar predictions in shallow water?'' in *Impact of Littoral Environmental Variability on Acoustic Predictions and Sonar Performance*, edited by N. Pace and F. Jensen (Lerici, Italy) (Kluwer Academic Publishers, Dordecht, The Netherlands).

Frisk, G. V., and Lynch, J. F. (**1984**). ''Shallow water waveguide characterization using the Hankel transform,'' J. Acoust. Soc. Am. **76**, 205–216.

Hamilton, E. L. (**1980**). ''Geoacoustic modeling of the seafloor,'' J. Acoust. Soc. Am. **68**, 313–339.

Holland, C. W., and Osler, J. (**2000**). ''High resolution geoacoustic inversion in shallow water: A joint time and frequency domain technique,'' J. Acoust. Soc. Am. **107**, 1263–1279.

Holland, C. W. (**2002**). ''Geoacoustic inversion for fine-grained sediments,'' J. Acoust. Soc. Am. **111**, 1560–1564.

Jensen, F. B., and Kuperman, W. A. (**1983**). ''Optimum frequency of propagation in shallow water environments,'' J. Acoust. Soc. Am. **73**, 813–819.

Menke, W. (**1989**). *Geophysical Data Analysis: Discrete Inverse Theory* (Academic, New York).

Porter, M. B. (**1991**). ''The KRAKEN normal mode program,'' SACLANTCEN Memorandum SM-245, SACLANT Undersea Research Centre, La Spezia.

Rubano, L. A. (**1980**). ''Acoustic propagation in shallow water over a low-velocity bottom,'' J. Acoust. Soc. Am. **67**, 1608–1613.

Siderius, M., Nielsen, P. L., Sellschopp, J., Snellen, S., and Simons, D. (**2001**). ''Experimental study of geo-acoustic inversion uncertainty due to ocean sound-speed fluctuations,'' J. Acoust. Soc. Am. **110**, 769–781.

Urick, R. J. (**1970**). ''Reverberation-derived scattering strength of the shallow sea bed,'' J. Acoust. Soc. Am. **48**, 392.

Weinberg, H., and Keenan, R. E. (**1996**). ''Gaussian ray bundles for modeling high-frequency propagation loss under shallow-water conditions,'' J. Acoust. Soc. Am. **100**, 1421–1431.

Westwood, E. K., and Vidmar, P. J. (**1987**). ''Eigenray finding and time series simulation in layered bottom ocean,'' J. Acoust. Soc. Am. **81**, 912–924.